Multi-modality Image Registration using the Decomposition Model

Mazlinda Ibrahim[1,a)] and Ke Chen[2,b)]

[1]*Department of Mathematics, Center for Defence Foundation Studies, National Defence University of Malaysia, 57000 Kuala Lumpur, Malaysia*
[2]*Centre for Mathematical Imaging Techniques and Department of Mathematical Sciences, The University of Liverpool, Liverpool L69 7ZL, United Kingdom.*

[a)]Corresponding author: mazlinda@upnm.edu.my
[b)]K.Chen@liv.ac.uk

Abstract. In medical image analysis, image registration is one of the crucial steps required to facilitate automatic segmentation, treatment planning and other application involving imaging machines. Image registration, also known as image matching, aims to align two or more images so that information obtained can be compared and combined. Different imaging modalities and their characteristics make the task more challenging. We propose a decomposition model combining parametric and non-parametric deformation for multi-modality image registration. Numerical results show that the normalised gradient field perform better than the mutual information with the decomposition model.

INTRODUCTION

A broad types of imaging machines in medical application makes registration of images from different modalities a challenging task. It is an open and active area of research because alignment of multi-modal images are complementary of each others. One of the common applications of multi-modality image registration is in the process of detection of the breast cancer. Several modalities such as MRI, mammography and ultrasound are combine in order to have an accurate measure of the cancerous tissues. The registration process has to deal with not only the geometric distortion caused by patient movements but the intensity distortion such as the bias field effect which commonly appears in MRI. In addition, what makes the task more difficult is non-existent of functional relation between the intensity values of the same object in different images. One of the remedies is to use landmark registration method where clinician identifies several corresponding feature points in images. However, this particular approach is time consuming, requires an expert to extract the points and there are some possibilities of mismatching of the points.

One of the commonly used similarity measure for multi-modality images is mutual information (MI). It was first introduced independently by Maes et al. in [1] and Viola and Wells in [2] and there is an assumption made based on the information contents. This particular measure aims to find a statistical intensity relationship between the reference and template images. When two images are aligned, the amount of share information is maximised. It has been successfully applied to the rigid and affine image registration. See [3, 4, 5] for more details. For the non-rigid image registration, the best implementation of MI is not trivial because it is a global measure, therefore its local estimation is difficult and using MI as the distance measure increasing the non-convexity of registration problem [6]. In [7], the authors provide a taxonomy for MI which summarises several variants of MI and their limitations.

Real images are often distorted by spatially varying intensity inhomogeneities. As such, MRI are affected by additive or multiplicative bias field. Image registration models based on mutual information are at disadvantages with the appearance of the bias field. In [8], the authors proposed an alternative measure known as normalised gradient field (NGF), a novel similarity measure for multi-modality image registration which is more reliable and robust than MI. NGF is based on the alignment of the edges in the reference and template images. In [9], NGF is used to register dynamic contrast enhance (DCE)-MRI with elastic image registration model.

In this paper, we propose the decomposition model [10] for multi-modality images using MI and NGF. The decomposition model is based on combining parametric and non-parametric models where we particularly choose cubic B-spline and linear curvature model by Fischer and Modersitzki [11, 12]. First, we introduce the mathematical background for mutual information and normalised gradient field as distance measure for image registration. Second, we review the decomposition model of parametric and non-parametric image registration using MI and NGF. Third, we present the numerical algorithm to solve these two models. Then, we present numerical tests and finally, we discuss and conclude the two models.

MULTI-MODALITY IMAGE REGISTRATION

In this section we introduce the mathematical background for mutual information as a distance measure in image registration. We recall the mathematical setting for image registration followed by the definition of mutual information and normalised gradient field.

Mathematical preliminaries for Image Registration: Given two images the reference R and template T where they are compactly bounded and support operator $T, R : \mathbb{R}^2 \rightarrow \mathbb{R}^+$. The image domain is denoted as $\Omega^h = [0, N_1] \times [0, N_2]$ and the pixel location is given by

$$\mathbf{x}_{i,j} = (x_{1,i}, x_{2,j}) \in \Omega^h, 0 \leq i \leq N_1, 0 \leq j \leq N_2$$

where $x_{1,i} = ih_1$, $x_{2,j} = jh_2$, h_1 and h_2 are pixel width and height and images R and T are of size $N_1 \times N_2$. For the ease of computation we use $h = h_1 = h_2$ and $N = N_1 = N_2$. We aim to align T and R such that the transform template image $T(\varphi)$ is aligned geometrically with R. The transformation φ is vector valued function where $\varphi : \mathbb{R}^2 \rightarrow \mathbb{R}^2$. For nonparametric image registration we can model the transformation φ as

$$\varphi(\mathbf{x}) = \mathbf{x} + \mathbf{u}(\mathbf{x}).$$

Mutual Information Distance Measure

The mutual information distance measure $\mathcal{D}^{MI}$ is defined by $\mathcal{D}^{MI} : \mathbb{R}^d \rightarrow \mathbb{R}$ where

$$\mathcal{D}^{MI}(T, R; \varphi) = -\int_{\mathbb{R}^2} p_{T(\varphi),R}(t, r) \log \frac{p_{T(\varphi),R}(t, r)}{p_{T(\varphi)}(t) p_R(r)} \, \mathrm{d}t \, \mathrm{d}r \tag{1}$$

where φ is the transformation $\varphi : \mathbb{R}^2 \rightarrow \mathbb{R}^2$ for two dimensional images. $p_{T(\varphi),R}(t, r)$ is the joint probability density. $p_{T(\varphi)}(t)$ and $p_R(r)$ are the marginal probability probabity density for the transformed template image and the reference image respectively. Mutual information is a measure of similarity between given images. When $T(\varphi)$ and R are aligned the information contain is maximal.

Normalised Gradient Field Distance Measure

The sum of the squared distance measure assumes the intensity values of R and the transformed template $T(\varphi)$ is equal. Meanwhile, mutual information made an assumption that there are statistical dependency between $T(\varphi)$ and R. A trade off between the SSD and MI is the normalised gradient field (NGF) distance measure where it is based on the alignment of the edges of R and $T(\varphi)$. The features in $T(\varphi)$ and R can be observed by the intensity changes which indicated by the gradient of $T(\varphi)$ and R. Since we are not interested in the magnitude of the gradient because there is no intensity relationship, we normalised the gradient with the magnitude of the gradient

$$\mathbf{n}T(\mathbf{x}) = \frac{\nabla T}{||\nabla T||_{\epsilon_T}}, \quad \mathbf{n}R(\mathbf{x}) = \frac{\nabla R}{||\nabla R||_{\epsilon_R}}$$

where

$$||\nabla T||_{\epsilon_T} = \sqrt{||\nabla T||^2 + \epsilon_T^2}, \quad ||\nabla R||_{\epsilon_R} = \sqrt{||\nabla R||^2 + \epsilon_R^2},$$

ϵ_T and ϵ_R are added into the calculation of NGF to overcome the problem when dividing by zero. Based on [8, 13], the values are given by

$$\epsilon_T = \frac{\eta}{V}\int_\Omega \|\nabla T(\mathbf{x})\|\,\mathrm{d}\Omega$$

where η is the estimated noise level and V is the volume of the domain Ω and similarly for ϵ_R. These parameters act as threshold values for the edges. When $\|\nabla T(\mathbf{x})\| > \epsilon_T$, it consider as an edges and when $\|\nabla T(\mathbf{x})\| < \epsilon_T$, it is consider as noise. For two vector $\mathbf{a}$ and $\mathbf{b}$, the dot product is of

$$\mathbf{a}\cdot\mathbf{b} = \|\mathbf{a}\|\|\mathbf{b}\|\cos\theta$$

and the cross product is

$$\|\mathbf{a}\times\mathbf{b}\| = \|\mathbf{a}\|\|\mathbf{b}\|\sin\theta.$$

where θ is the angle between $\mathbf{a}$ and $\mathbf{b}$. Then,

$$\cos\theta = \frac{\mathbf{a}\cdot\mathbf{b}}{\|\mathbf{a}\|\|\mathbf{b}\|} \;\; and \;\; \sin\theta = \frac{\|\mathbf{a}\times\mathbf{b}\|}{\|\mathbf{a}\|\|\mathbf{b}\|}$$

Based on the dot and cross products of two vectors, we can defined the NGF similarity measure as

$$\mathcal{D}^{NGFc}(T,R) = \frac{1}{2}\int_\Omega d^c(T,R)\,\mathrm{d}\Omega, \quad d^c(T,R) = \|\mathbf{n}T(\mathbf{x})\times\mathbf{n}R(\mathbf{x})\|^2$$

and

$$\mathcal{D}^{NGFd}(T,R) = -\frac{1}{2}\int_\Omega d^d(T,R)\,\mathrm{d}\Omega, \quad d^d(T,R) = (\mathbf{n}T(\mathbf{x})\cdot\mathbf{n}R(\mathbf{x}))^2$$

which are equivalent from an optimisation point of view [8, 13]. In this paper we will use

$$\mathcal{D}^{NGF}(T,R) = \int_\Omega 1-(\mathbf{n}T(\mathbf{x})^T\mathbf{n}R(\mathbf{x}))^2\,\mathrm{d}\Omega$$

as the normalised gradient field distance measure for image registration.

A DECOMPOSITION MODEL FOR IMAGE REGISTRATION

A general framework for image registration is given by

$$\min_{\varphi(\mathbf{x})} \mathcal{J}(T,R,\varphi(\mathbf{x})) = \mathcal{D}(T,R,\varphi(\mathbf{x})) + \gamma\mathcal{S}(\varphi(\mathbf{x}))$$

where $\mathcal{D}(T,R,\varphi(\mathbf{x}))$ is a similarity measure which quantified how much T and R are different, $\mathcal{S}(\varphi(\mathbf{x}))$ is the smoothness or regularisation term and γ is the regularisation parameter. The decomposition model of parametric and non-parametric image registration [10] decomposes the displacement field as

$$\varphi(\mathbf{x}) = \mathbf{u}_p(\mathbf{x}) + \mathbf{u}_{np}(\mathbf{x})$$

where $\mathbf{u}_p(\mathbf{x})$ and $\mathbf{u}_{np}(\mathbf{x})$ are the displacement field from parametric and non-parametric model respectively. In [10], the authors recommend this particular choice:

$$\varphi(\mathbf{x}) = \mathbf{u}_{cubic\ B\text{-}spline} + \mathbf{u}_{FMC}$$

where $\mathbf{u}_{cubic\ B\text{-}spline}$ is the cubic B-spline based model [14] and $\mathbf{u}_{FMC}$ is Fischer and Modersitzki linear curvature model [11, 12]. The functional minimisation problem for the decomposition model is given by

$$\min_{\mathbf{u}_{cubic\ B\text{-}spline},\mathbf{u}_{FMC}} \mathcal{J}_{\gamma_p,\gamma_{np}} = \mathcal{D}(T,R,\mathbf{u}_{cubic\ B\text{-}spline},\mathbf{u}_{FMC}) + \gamma_p\mathcal{S}^{TP}(\mathbf{u}_{cubic\ B\text{-}spline}) + \gamma_{np}\mathcal{S}^{FMC}(\mathbf{u}_{FMC}). \tag{2}$$

The regularisation terms for equation (2) are as follows:

$$\mathcal{S}^{TP}(\mathbf{u}) = \sum_{l=1}^{2} \int_{\Omega} (u_{l,x_1x_1})^2 + (2u_{l,x_1x_2})^2 + (u_{l,x_2x_2})^2)\, \mathrm{d}\Omega, \mathcal{S}^{FMC}(\mathbf{u}) = \int_{\Omega} (\Delta u_1)^2 + (\Delta u_2)^2\, \mathrm{d}\Omega.$$

where $u_{l,x_1x_1} = \frac{\partial^2 u_l}{\partial x_1^2}$ and similarly for u_{l,x_1x_2} and u_{l,x_2x_2}. For multi-modality images, we will used two distance measure

$$\mathcal{D}^{MI}(T, R; \varphi) = \int_{\Omega} p_{T(\varphi),R}(t, r) \log \frac{p_{T(\varphi),R}(t, r)}{p_{T(\varphi)}(t) p_R(r)}\, \mathrm{d}t\, \mathrm{d}r, \mathcal{D}^{NGF}(T, R; \varphi) = \int_{\Omega} 1 - (\mathbf{n}T(T(\varphi)))^T \mathbf{n}R(\mathbf{x}))^2\, \mathrm{d}\Omega$$

as discussed in the previous section. Denote $\mathbf{u}_{cubic\ B\text{-}spline} = \mathbf{u}_p$ and $\mathbf{u}_{FMC} = \mathbf{u}_{np}$ for a more general framework. Since the parametric displacement fields $\mathbf{u}_p$ are depending on a certain number parameter of α, then we will minimise (2) with respect to the parameters α.

Problem (2) can be solved by alternating minimisation of two subproblems

$$\min_{\alpha} \mathcal{J}^I_{\gamma_p} = \mathcal{D}(T, R, \mathbf{u}_p(\mathbf{x}, \alpha), \mathbf{u}_{np}) + \gamma_p \mathcal{S}^{TP}(\mathbf{u}_p(\mathbf{x}, \alpha)) \tag{3}$$

and

$$\min_{\mathbf{u}} \mathcal{J}^{II}_{\gamma_p} = \mathcal{D}(T, R, \mathbf{u}_p(\mathbf{x}, \alpha), \mathbf{u}_{np}) + \gamma_{np} \mathcal{S}^{FMC}(\mathbf{u}_{np}(\mathbf{x})). \tag{4}$$

We use the discretise than optimise scheme for numerical solutions. At the kth iteration, the alternate update are done as follows:

Fixing $\mathbf{u}^{(k)}_{np}(\mathbf{x})$, we solve problem (3):

$$\begin{aligned} \mathbf{u}^{(k+1)}_p(\mathbf{x}, \alpha) \leftarrow \min_{\alpha} \mathcal{J}^I_{\gamma_p} &= \sum_{i,j=0}^{N-1} \mathcal{D}(T(\mathbf{u}_p(\mathbf{x}_{i,j}, \alpha) + \mathbf{u}_{np}(\mathbf{x}_{i,j})), R(\mathbf{x}_{i,j})) + \gamma_p \mathcal{S}^{TP}(\mathbf{u}_p(\mathbf{x}_{i,j}, \alpha)) \\ &= \sum_{i,j=0}^{N-1} \mathcal{D}(T(\mathbf{u}_p(\mathbf{x}_{i,j}, \alpha) + \mathbf{u}_{np}(\mathbf{x}_{i,j})), R(\mathbf{x}_{i,j})) + \gamma_p \sum_{l=1}^{2} \sum_{i,j=0}^{N-1} \left(u_{p,l,x_1x_1}(\mathbf{x}_{i,j}, \alpha)\right)^2 \\ &+ 2\left(u_{p,l,x_1x_2}(\mathbf{x}_{i,j}, \alpha)\right)^2 + \left(u_{p,l,x_2x_2}(\mathbf{x}_{i,j}, \alpha)\right)^2 \end{aligned} \tag{5}$$

Fixing $\mathbf{u}^{(k+1)}_p(\mathbf{x}, \alpha)$, we solve problem (4):

$$\begin{aligned} \mathbf{u}^{(k+1)}_{np}(\mathbf{x}) \leftarrow \min_{\mathbf{u}_{np}(\mathbf{x})} \mathcal{J}^I_{\gamma_{np}} &= \sum_{i,j=0}^{N-1} \mathcal{D}(T(\mathbf{u}_p(\mathbf{x}_{i,j}, \alpha) + \mathbf{u}_{np}(\mathbf{x}_{i,j})), R(\mathbf{x}_{i,j})) + \gamma_{np} \mathcal{S}^{FMC}(\mathbf{u}_{np}(\mathbf{x}_{i,j})) \\ &= \sum_{i,j=0}^{N-1} \mathcal{D}(T(\mathbf{u}_p(\mathbf{x}_{i,j}, \alpha) + \mathbf{u}_{np}(\mathbf{x}_{i,j})), R(\mathbf{x}_{i,j}))\gamma_{np} \sum_{l=1}^{2} \sum_{i,j=0}^{N-1} \Big[-4\mathbf{u}_{np,l}(\mathbf{x}_{i,j}) + \mathbf{u}_{np,l}(\mathbf{x}_{i+1,j}) \\ &+ \mathbf{u}_{np,l}(\mathbf{x}_{i-1,j}) + \mathbf{u}_{np,l}(\mathbf{x}_{i,j+1}) + \mathbf{u}_{np,l}(\mathbf{x}_{i,j-1}) \Big]^2 \end{aligned} \tag{6}$$

To solve (5), $\mathbf{u}_p(\mathbf{x}, \alpha)$ are defined by the cubic B-splines with coefficient α:

$$u_{p,1}(\mathbf{x}, \alpha_1) = \sum_{i,j} B_{i,j}(\mathbf{x}) \alpha_{1,i,j}, u_{p,2}(\mathbf{x}, \alpha_2) = \sum_{i,j} B_{i,j}(\mathbf{x}) \alpha_{2,i,j}$$

where $\alpha = (\alpha_1, \alpha_2)^T$, is the lattice of control points which are the parameters for the cubic B-spline model. $B_{i,j}(\mathbf{x})$ are given by

$$B_{i,j}(\mathbf{x}) = \begin{cases} B_l(\mu) B_m(\nu), & i = \widetilde{i} + l, j = \widetilde{j} + m, \text{ for } l, m = 0, 1, 2, 3; \\ 0, & \text{elsewhere.} \end{cases}$$

where $B_l(\mu)$ and $B_m(\nu)$ are cubic B-spline basis functions as follows:

$$\begin{aligned} B_0(\mu) &= (1-\mu)^3/6, \\ B_1(\mu) &= (3\mu^3 - 6\mu^2 + 4)/6, \\ B_2(\mu) &= (-3\mu^3 + 3\mu^2 + 3\mu + 1)/6, \\ B_3(\mu) &= \mu^3/6, \end{aligned} \tag{7}$$

$\widetilde{i} = \lfloor \frac{x_1}{\delta x_1} \rfloor - 1, \widetilde{j} = \lfloor \frac{x_2}{\delta x_2} \rfloor - 1, \mu = \frac{x_1}{\delta x_1} - \lfloor \frac{x_1}{\delta x_1} \rfloor$ and $\nu = \frac{x_2}{\delta x_2} - \lfloor \frac{x_2}{\delta x_2} \rfloor$. The spacing of the control points δx_1 and δx_2 are the predefined parameters. Next is to solve (6) iteratively using LBFGS method. See [10] for more details.

NUMERICAL RESULTS

We use three sets of tests to show the performance of the decomposition model for multi-modality images. In Test 1, we have a reference image from photon density weighted MRI and a template image which is coming from T2-MRI. For Test 2, we have synthetic images from [15] to illustrate the type of images where mutual information and decomposition model are at disadvantages. We obtain a good result using normalised gradient field and the decomposition model for Test 2. Meanwhile, for Test 3, we are using images from [16] to illustrate case where both models fail to deliver good registration results.

Test 1: Photon Density Weighted MRI and T2-MRI

The results for mutual information and decomposition model for Test 1 are shown in Figure 1. In Figure 1, we can observe that the decomposition model with mutual information as the distance measure are able to solve real medical image where the reference and template images are coming from photon density weighted MRI and T2-MRI respectively. We show the results for Test 1 using normalised gradient field in Figure 2. The transformed template image for normalised gradient field and the decomposition model is shown in Figure 2 (b). We have an acceptable level of the transformed template image where it appears similar with the reference image except at the middle right part of the brain.

Test 2: Synthetic Images

In Test 2, we aim to illustrate type of images where mutual information and the decomposition model fail to deliver good registration results. Since mutual information used the statistical dependency of the intensity values between the reference and template images, the model fails to register this type of problem because only the reference image has the square object inside the circle. However, we have a good result using normalised gradient field as shown in Figure 4.

Test 3: Bias Field Registration

Bias field or intensity inhomogeneities is a common problems in medical image analysis where some part of the same object in the image appears to become darker than the rest of the object. It is a very common problem in MRI. In Figure 5, we show the results of mutual information with strong bias field in the template image. Normalised gradient field and the decomposition model also fail to register Test 3 as depicted in Figure 6. We can see that in the figure, the most outer boundary of the brain in transformed template image is not aligned with the one in reference image.

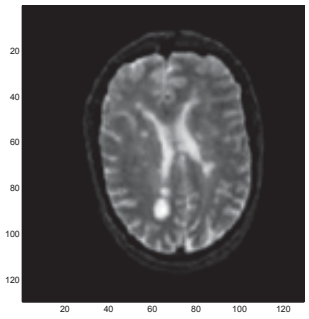

(a) T, *with* $\mathcal{D}^{MI}(T,R) = -0.5966$

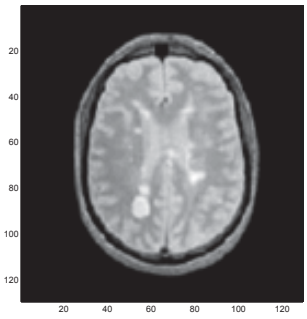

(b) R

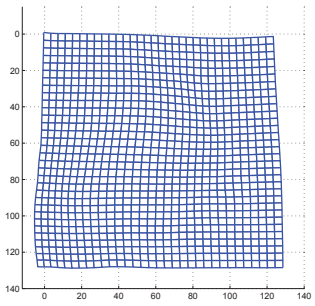

(c) $\varphi(\mathbf{x})$

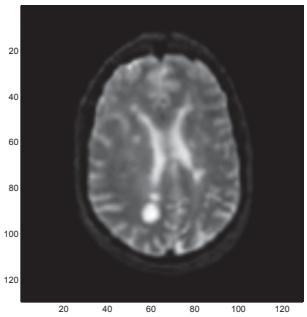

(d) $T(\varphi(\mathbf{x}))$ *with* $\mathcal{D}^{MI}(T(\varphi(\mathbf{x})),R) = -0.8013$

FIGURE 1. Test 1: Results of mutual information as the distance measure with the decomposition model for multi-modality images. We can see that the model delivers a good alignment between the transformed template image in (d) and the reference image in (b).

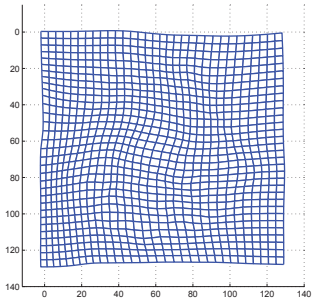

(a) $\varphi(\mathbf{x})$

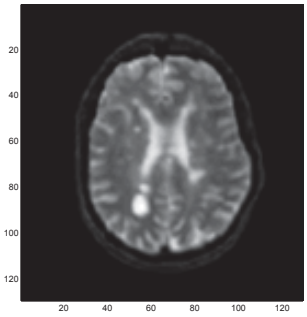

(b) $T(\varphi(\mathbf{x}))$ *with* $\mathcal{D}^{MI}(T(\varphi(\mathbf{x})),R) = -0.9709$

FIGURE 2. Test 1: Results of normalised gradient as the distance measure with the decomposition model for multi-modality images. The resulting transformed template in (b) is in alignment with the reference image except at the middle part of the brain.

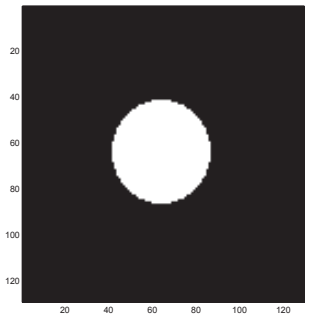

(a) T *with* $\mathcal{D}^{MI}(T,R) = -0.2472$

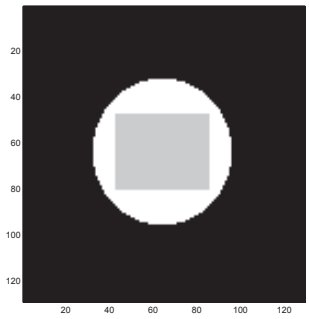

(b) R

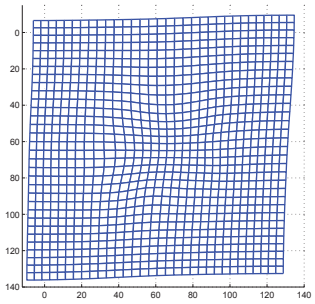

(c) $\varphi(\mathbf{x})$

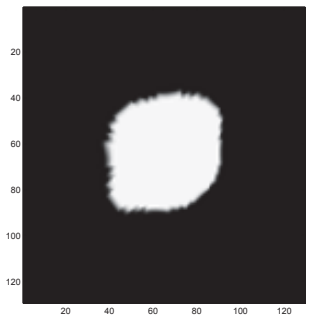

(d) $T(\varphi(\mathbf{x}))$ *with* $\mathcal{D}^{MI}(T(\varphi(\mathbf{x})),R) = -0.3777$

FIGURE 3. Test 2: Results of mutual information as the distance measure with the decomposition model for multi-modality images. We can see that the model fails the deformed the circle in the template image in (a) due to the existence of the inner square in the reference image (b).

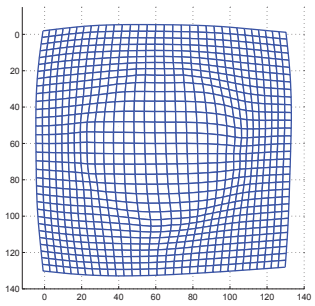

(a) $\varphi(\mathbf{x})$

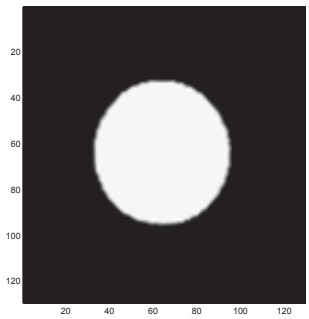

(b) $T(\varphi(\mathbf{x}))$ *with* $\mathcal{D}^{MI}(T(\varphi(\mathbf{x})),R) = -0.4902$

FIGURE 4. Test 2: Results of normalised gradient as the distance measure with the decomposition model for multi-modality images. We can see the model is able to solve this particular problem.

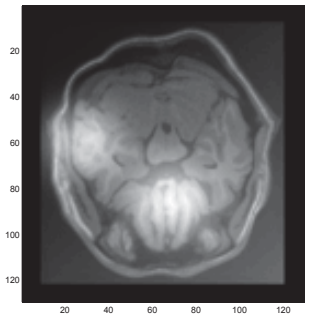

(a) T *with* $\mathcal{D}^{MI}(T, R) = -0.5710$

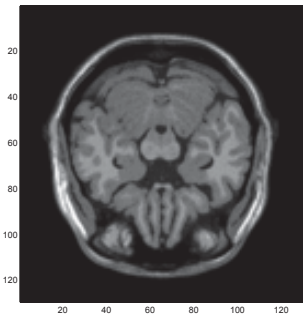

(b) R

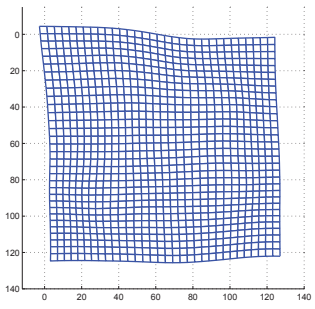

(c) $\varphi(\mathbf{x})$

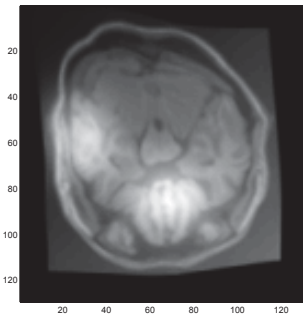

(d) $T(\varphi(\mathbf{x}))$ *with* $\mathcal{D}^{MI}(T(\varphi(\mathbf{x})), R) = -0.5742$

FIGURE 5. Test 3: Results of mutual information as the distance measure with the decomposition model for multi-modality images. We can see that the model fails to register the template with the reference image due to the strong bias field in (a).

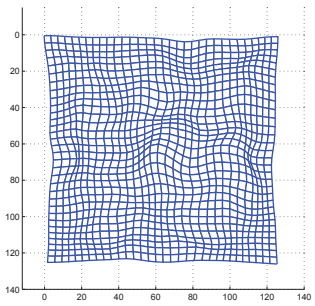

(a) $\varphi(\mathbf{x})$

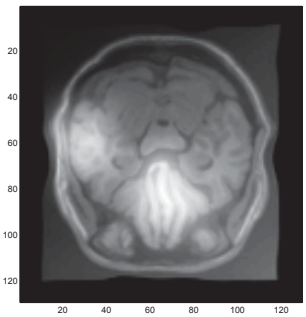

(b) $T(\varphi(\mathbf{x}))$ *with* $\mathcal{D}^{MI}(T(\varphi(\mathbf{x})), R) = -0.6773$

FIGURE 6. Test 3: Results of normalised gradiet field as the distance measure with the decomposition model for multi-modality images. We can see that the model fails to register the template with the reference image due to the strong bias field in (a).

CONCLUSIONS

From the numerical tests, we can observe that the normalised gradient field and decomposition model work better than the mutual information. However both models are at disadvantages when there are strong bias field in the images.

ACKNOWLEDGEMENTS

The research and writing of this work was partially carried out under UPNM short term grants: UPNM/2016/GPJP/3/SG/3 and UPNM/2016/GPJP/3/SG/4.

REFERENCES

[1] F. Maes, A. Collignon, D. Vandermeulen, G. Marchal, and P. Suetens, IEEE T. Med. Imaging **16**, 187–198 (1997).
[2] P. Viola and W. M. Wells III, Int. J. Comput. Vision **24**, 137–154 (1997).
[3] J. P. Pluim, J. B. Maintz, and M. A. Viergever, IEEE T. Med. Imaging **22**, 986–1004 (2003).
[4] A. Rangarajan, H. Chui, and J. S. Duncan, Medical Image Analysis **3**, 425–440 (1999).
[5] R. Shekhar and V. Zagrodsky, IEEE Transactions on Medical Imaging **21**, 9–22 (2002).
[6] M. P. Heinrich, M. Jenkinson, M. Bhushan, T. Matin, F. V. Gleeson, S. M. Brady, and J. A. Schnabel, Med. Image Anal. **16**, 1423–35 (2012).
[7] T. Borvornvitchotikarn and W. Kurutach, "A taxonomy of mutual information in medical image registration," in *2016 International Conference on Systems, Signals and Image Processing (IWSSIP)* (IEEE, 2016), pp. 1–4.
[8] E. Haber and J. Modersitzki, "Beyond mutual information: A simple and robust alternative," in *Bildverarbeitung fr die Medizin 2005* (Springer Berlin Heidelberg, 2005), pp. 350–354.
[9] E. Hodneland, A. Lundervold, J. Rrvik, and A. Z. Munthe-Kaas, Comput. Med. Imag. Grap. **38**, 202–210 (2014).
[10] M. Ibrahim and K. Chen, "A composition model combining parametric transformation and non-parametric deformation for effective image registration," in *SIAM Conference on Imaging Science* (2014).
[11] B. Fischer and J. Modersitzki, in *Computational Science ICCS 2002* (Springer, 2002), pp. 202–206.
[12] B. Fischer and J. Modersitzki, J. Math. Imaging Vis. **18**, 81–85 (2003).
[13] E. Haber and J. Modersitzki, "Intensity gradient based registration and fusion of multi-modal images," in *Medical Image Computing and Computer-Assisted Intervention MICCAI 2006* (Springer Berlin Heidelberg, 2006), pp. 726–733.
[14] D. Rueckert, L. I. Sonoda, C. Hayes, D. L. Hill, M. O. Leach, and D. J. Hawkes, IEEE T. Med. Imaging **18**, 712–21 (1999).
[15] N. Chumchob and K. Chen, Numer. Meth. Part. D. E. **28**, 1966–1995 (2012).
[16] A. Myronenko and S. Xubo, IEEE Transactions on Medical Imaging **29**, 1882–1891 (2010).